FLIGHT TEST VALIDATION OF MODELING FOR AERIAL REFUELLING

J. Beck, O. Heller[1], E. Özger
EADS Deutschland GmbH, Military Air Systems, 81663 Munich, Germany
[1]Eurocopter, 13725 Marignane Cedex, France

OVERVIEW

This paper describes the flight-mechanic modelling of the interactions between an aerial tanker and a considerably smaller receiving aircraft. Several models of the description of the tanker's trailing vortices are presented. By means of an averaging scheme, these models are then used for determining the additional velocities and angular rates, which are induced at the receiving aircraft's centre of gravity. A comparison with flight test data for the aerial refuelling of a modern high-performance aircraft shows, that all the models considered exhibit similar suitability for the prediction of induced pitch and yaw moments. However, for the rolling moment calculation the *Adapted Vortex Models* is best suited for flight-mechanic considerations and control law design.

NOMENCLATURE

a	axis along t/4-line
b	wing span
c.g.	centre of gravity
c_l	coefficient for rolling moment
c_m	coefficient for pitching moment
c_n	coefficient for yawing moment
c_X	coefficient for x-force
c_Y	coefficient for y-force
c_Z	coefficient for z-force
f_i	weighting function
F_{FT}	measured inertial force
F_{Intake}	intake force
F_{nozzle}	nozzle force
g	acceleration due to gravity
l_x	airplane length
l_z	airplane height
m	airplane mass
M_{FT}	measured inertial force
M_{Intake}	intake moment
M_{nozzle}	nozzle moment
p	parameter (Smooth Blending Profile)
r_c	vortex core radius
r	distance from point to horseshoe vortex
s	half-span
V_θ	induced velocity
V	air speed
V_{TAS}	true air speed
W	induced wind speed
Δx	longitudinal distance
α	angle of attack
β	angle of sideslip
β_0	parameter (Smooth Blending Profile)
β_i	parameter (Smooth Blending Profile)
δ	symmetric flap position
ε	parameter for vortex decay
ε	leading edge position
η	canard position
Γ_0	maximum circulation of vortex
ρ	air density
ξ	differential flap position
ζ	rudder position
τ	time

Indices:

ADM	based on aerodynamic model ADM
FT	derived from flight-test data
model	based on vortex model

1. INTRODUCTION

In the recent years, the topic of aerial refuelling has attracted quite some attention. This was mainly in the context of UAVs, where autonomous refuelling would further improve the capability to perform long-time missions [1][2][3][4] . However, not only for uninhabited platforms, but also human-piloted aircraft, an automatic refuelling capability can be considered advantageous, as this would aid in reducing pilot workload.

Whatever the motivation, any control law and autopilot design requires a sufficiently precise description of the aerodynamic forces and moments. During this refuelling process, the interaction between the flow fields of tanker and receiver aircraft will induce additional moments and forces on both aircraft.

During a literature research, some models for the flow field in close proximity to an aircraft have been found. Additionally, schemes for the determination of the induced forces and moments are available, as well. However, a comparison of predicted effects with flight test data seems to be missing. This paper aims to close that gap.

In the following chapters, first the aerial refuelling process is described, for which the modelling has been analysed.
Then different aerodynamic models are outlined, which are used to determine the velocity field of an aircraft's horseshoe vortex. Using the velocity field description, an averaging scheme is described. This scheme to calculate the angular rates induced at the receiving aircraft..
These angular rates are then compared to those determined during flight tests. Based on this comparison, the suitability of the different models for the flight mechanic description is assessed.

2. DESCRIPTION OF AERIAL REFUELLING PROCESS

This work deals with aerial refuelling performed with the probe-and-drogue system. An aerial tanker a/c (e.g. A310 MRTT) extends a hose from a pod at the outboard end of the wing. At the end of the hose there is a basked, which the receiver aircraft needs to capture with its refuelling probe. The ensuing geometry is shown in figs. 1 and 2.

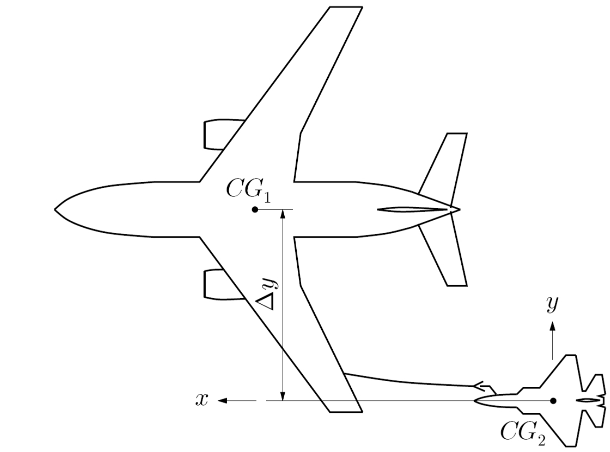

FIG 2. Aerial Refuelling: Top View

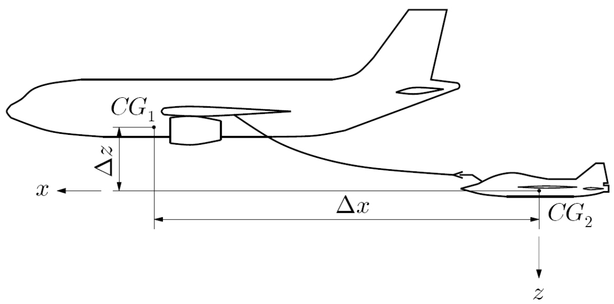

FIG 1. Aerial Refuelling: Side View

During the refuelling the two aircraft fly in close proximity to each other. Therefore they mutually influence each other's flow field and thus induce additional forces and moments.
The tanker aircraft's flaps require a spanwise position for the refuelling pod, which is relatively far outboard. Unfortunately, in this region the trailing vortices will develop. Therefore the tanker aircraft's flow field considerably influences the receiving aircraft.
In the present case, the receiving aircraft is significantly smaller and lighter than the tanker aircraft. Therefore it is considered acceptable to neglect the influence of the receiver on the tanker. Of course, for buddy-buddy refuelling this assumption is not valid.

3. MODELLING

3.1. Aerodynamic Models

The most basic description of the velocities induced by a horseshoe vortex is the well-known Helmholtz-Profile

$$(1)\quad V_\theta = \frac{\Gamma_0}{2\pi r}$$

V_θ is the induced velocity at the point p in the vortex plane, while r is the point's distance to the vortex and Γ_0 the maximum circulation of the vortex.

Assuming an elliptic lift distribution and flight at 1 g the circulation is

$$(2)\quad \Gamma_0 = \frac{4mg}{\pi \rho b V}.$$

m ist the airplane mass, g the acceleration due to gravity, ρ the air density, b the wing span and V the airspeed. Hallock and Burnham [5] improved (1) by including the vortex core radius r_c :

$$(3)\quad V_\theta = \frac{\Gamma_0}{2\pi}\frac{r}{r^2 + r_c^2}$$

The core radius is in the range of 1-6% of the wing span, depending on the aircraft. Similarly, the *Lamb–Oseen-Model* [6] considers the core radius, but accounts for the reduced influence of the core region with increasing distance from the vortex

$$(4)\quad V_\theta = \frac{\Gamma_0}{2\pi r}\left[1 - e^{-1.2526\left(\frac{r}{r_c}\right)^2}\right]$$

The *Modified Horseshoe Vortex Profile*, proposed by Venkataramanan and Dogan [7], considers the decay of the vortex, but not its core radius:

$$(5)\quad V_\theta = \frac{\Gamma_0}{2\pi r}\left[1 - e^{-\frac{r^2}{4\varepsilon\tau}}\right]$$

ε is the parameter for the decay of the vortex, while τ is the time since the vortex left the wing. For constant flight speed V_{TAS} and a longitudinal distance Δx between tanker and receiver, the time is

$$(6)\quad \tau = \frac{\Delta x}{V_{TAS}}$$

The *Rankine-Profile* uses the *Helmholtz-Profile*, but distinguishes between regions within and outside of the vortex core:

$$(7)\quad V_\theta = \frac{\Gamma_0}{2\pi}\frac{r}{r_c^2} \quad \text{for } r \le r_c$$

$$(8)\quad V_\theta = \frac{\Gamma_0}{2\pi r} \quad \text{for } r > r_c$$

The Adapted Vortex Profile, put forward by Proctor [8], is based on LIDAR-measurements:

$$(9)\quad V_\theta = 1.4\frac{\Gamma_0}{2\pi}\left[1 - e^{-10\left(\frac{r_c}{b}\right)^{0.75}}\right]\left[1 - e^{-1.2526\left(\frac{r}{r_c}\right)^2}\right] \quad \text{for } r \le r_c$$

$$(10)\quad V_\theta = \frac{\Gamma_0}{2\pi}\left[1 - e^{-10\left(\frac{r}{b}\right)^{0.75}}\right] \qquad \text{for } r > r_c$$

Winkelmans et al [9] developed the *Smooth Blending Profile* as an adaptation of the *Adapted Vortex Profile*:

$$(11)\quad V_\theta = \frac{\Gamma_0}{2\pi}\left[1 - \exp\left(\frac{\beta_i\left(\frac{r}{b}\right)^2}{\left[1+\left\{\left(\frac{\beta_i}{\beta_0}\right)\left(\frac{r}{b}\right)^{5/4}\right\}^p\right]^{1/p}}\right)\right]$$

The parameters are given as

$$\beta_0 = 10\ ,\ \beta_i = \beta_0\left(\frac{b}{r_c}\right)^{5/4}\ ,\ \ p = [1....4]$$

3.2. Flight Dynamic Modelling

3.2.1. Averaging Method

The trailing vortices of an aircraft create a highly turbulent, non-linear flow field. Therefore it is not possible to apply the well-known equations with airspeed, angle of attack and angle of sideslip for the determination of the aerodynamic forces acting on an airplane flying in these disturbed surroundings.

However, in the equations of motion the influence of wind is taken into account by induced velocities at the aircraft's c.g.. Using this, it is possible to model the influence of the wake onto the refuelling aircraft.
In order to determine those velocities, first the wind velocities are first determined by means of one of the above vortex models and then averaged along x- and z-axes and the wing's quarter-cord line. This process supplies the velocities induced at the aircraft's c.g.

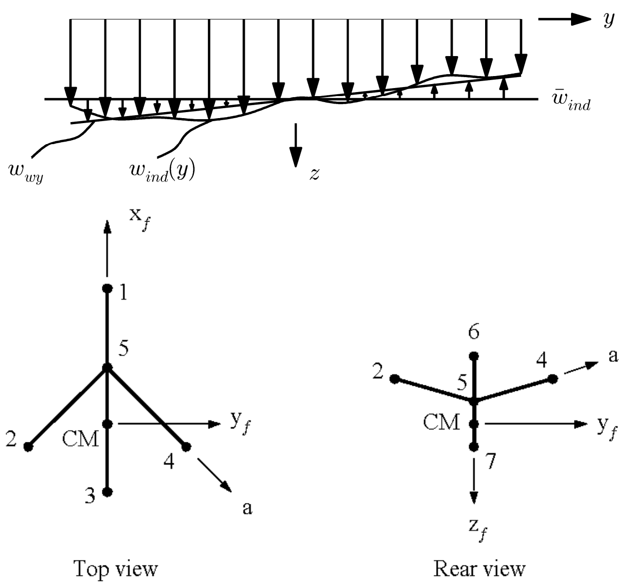

FIG 4. Characteristic aircraft lines

When we assume, that the induced wind velocities are distributed linearly around the c.g., wind gradients can be approximated as well (FIG 3).

As mentioned before, the velocities are averaged along the aircraft's characteristic lines, the x- and the z-axis and the wing's quarter-chord line, shown in FIG 4. For this we integrate the induced velocities' x-component along the line 6-CM, CM-7, 2-5 and 5-4:

$$(12)\quad \begin{aligned} W_{xy1} &= \frac{1}{b/2}\int_{a=-b/2}^{0} f_y(a)\, W_x\, da \\ W_{xy2} &= \frac{1}{b/2}\int_{a=0}^{b/2} f_y(a)\, W_x\, da \\ W_{xz1} &= \frac{1}{l_{z1}}\int_{z=l_{z1}}^{0} f_{z1}(z)\, W_x\, dz \\ W_{xz2} &= \frac{1}{l_{z2}}\int_{z=0}^{-l_{z2}} f_{z2}(z)\, W_x\, dz \end{aligned}$$

Here f_i are weighting factors, which will be described in the following sections.

On basis of (12) we can determine the resulting averaged velocity in the x-direction, induced at the c.g. as:

$$(13)\quad W_{x,ind} = \frac{W_{xy1} + W_{xy2} + W_{xz1} + W_{xz2}}{4}$$

The calculation of the components in direction of the y- and z-axes can be performed analogously.

Under the assumption of linear wind distribution along the aircraft's characteristic lines, the wind gradients can be calculated as:

$$(14)\quad \begin{aligned} \frac{\partial W_x}{\partial y} &= \frac{W_{xy2} - W_{xy1}}{b} & \frac{\partial W_x}{\partial z} &= \frac{W_{xz2} - W_{xz1}}{l_z} \\ \frac{\partial W_y}{\partial x} &= \frac{W_{yx1} - W_{yx2}}{l_x} & \frac{\partial W_y}{\partial z} &= \frac{W_{yz2} - W_{yz1}}{l_z} \\ \frac{\partial W_z}{\partial x} &= \frac{W_{zx1} - W_{zx2}}{l_x} & \frac{\partial W_z}{\partial y} &= \frac{W_{zy2} - W_{zy1}}{b} \end{aligned}$$

with aircraft length l_x, span b and the aircraft height l_z.

3.2.2. Weighting Schemes

When calculating the average velocities, the induced velocities along the x- and z-axis and along the quarter-chord line are weighted the same by using. f_i=1, i.e. all velocities contribute to the same degree, regardless of where it is induced.

However, when determining the wind gradients different

weighting schemes are possible. When we weight the induced velocities as a function of distance to the c.g. , the resulting wind gradients change, as shown in FIG 5. Venkataramanan and Dogan [7] showed that the weighting has a crucial importance for the accuracy of the procedure.
The following 5 sections describe the different schemes, which were employed in course of this work.

FIG 5. Influence of weighting method

3.2.2.1. Constant weighting

The simplest case is the uniform weighting. The weighting factor is constant, in our case f_i=1. The calculation of the wind gradient is analogous to that for the averaged velocities.

3.2.2.2. Linear weighting from 0 to 1

By applying a non-constant weighting, it is possible to consider the influence of the induced velocity on the induced angular rate. This influence increases as the distance between the induction point to the aircraft c.g. increases. Therefore the weighting factors must increase linearly with increasing distance from the c.g..

$$\text{(15)}\quad f_{x1} = \frac{|x|}{l_{x1}} \qquad f_{z1} = \frac{|z|}{l_{z1}}$$
$$f_{x2} = \frac{|x|}{l_{x2}} \qquad f_{z2} = \frac{|z|}{l_{z2}}$$
$$f_y = \frac{|a|}{b/2}$$

3.2.2.3. Linear weighting from 1 to 2

In the case of the linear weighting from 0 to 1 , the points close to the c.g. contribute only insignificantly to the resulting induced angular rate. Applying a weighting from 1 to 2 takes these points into account as well, while the more distant points still have a greater effect.

$$\text{(16)}\quad f_{x1} = 1+\frac{|x|}{l_{x1}} \qquad f_{z1} = 1+\frac{|z|}{l_{z1}}$$
$$f_{x2} = 1+\frac{|x|}{l_{x2}} \qquad f_{z2} = 1+\frac{|z|}{l_{z2}}$$
$$f_y = 1+\frac{|a|}{b/2}$$

3.2.2.4. Linear weighting starting from 0

Except for the lateral dimension, very few airplanes are symmetrical w.r.t the c.g. This is not taken into account with the previous weighting schemes. For the present linear weighting starting from 0, the weighting factors are defined in reference to the biggest length in each respective dimension.

$$\text{(17)}\quad f_{x1} = \frac{|x|}{\max(l_{x1}, l_{x2})} \qquad f_{z1} = \frac{|z|}{\max(l_{z1}, l_{z2})}$$
$$f_{x2} = \frac{|x|}{\max(l_{x1}, l_{x2})} \qquad f_{z2} = \frac{|z|}{\max(l_{z1}, l_{z2})}$$
$$f_y = \frac{|a|}{b/2}$$

3.2.2.5. Linear weighting starting from 1

Analogously to the linear weighting from 1 to 2 (sec. 3.2.2.3) the present scheme considers points close to the c.g. for the determination of the angular rates, while respecting the different dimensions w.r.t. the aircraft c.g.

$$\text{(18)}\quad f_{x1} = 1+\frac{|x|}{\max(l_{x1}, l_{x2})} \qquad f_{z1} = 1+\frac{|z|}{\max(l_{z1}, l_{z2})}$$
$$f_{x2} = 1+\frac{|x|}{\max(l_{x1}, l_{x2})} \qquad f_{z2} = 1+\frac{|z|}{\max(l_{z1}, l_{z2})}$$
$$f_y = 1+\frac{|a|}{b/2}$$

3.2.3. Angular Rates

The properties calculated in the previous sections allow determination of the angular rates induced by the tanker's wake vortex as :

$$\text{(19)}\quad p_{ind} = \frac{\partial W_z}{\partial y} - \frac{\partial W_y}{\partial z}$$
$$q_{ind} = \frac{\partial W_x}{\partial z} - \frac{\partial W_z}{\partial x}$$
$$r_{ind} = \frac{\partial W_y}{\partial x} - \frac{\partial W_x}{\partial y}$$

In general an aircraft's length (x-direction) and span (y-direction) is considerably larger than its height (z-direction). Therefore (19) can be approximated by:

$$p_{ind} = \frac{\partial W_z}{\partial y}$$

$$\text{(20)} \quad q_{ind} = -\frac{\partial W_z}{\partial x}$$

$$r_{ind} = \frac{\partial W_y}{\partial x} - \frac{\partial W_x}{\partial y}$$

Venkataramanan and Dogan [7] stated that for their tanker-receiver combination (20) gave actually better results than (19).

4. COMPARISON WITH FLIGHT TEST DATA

The above presented method to compute the induced angular rates has been developed Venkataramanan and Dogan [7] and has been validated by wind tunnel tests. As the tanker-receiver airplane combination used in the frame of our studies differs from the one chosen by Venkataramanan and Dogan [7], we validated the vortex model results by comparing them to available flight test data.

4.1. Flight Test Data for Aerial Refuelling

The flight test data was acquired during the aerial refuelling of an EF2000 Typhoon by a KC-135.

The data includes angle-of-attack, angular rates, velocities and force and moment coefficients, both from aircraft dynamics and the current aerodynamic model (in a body-fixed reference system).

The force and moment coefficients from the aircraft dynamics (c_{XFT}, c_{YFT}, c_{ZFT}, c_{lFT}, c_{mFT}, c_{nFT}) are derived from the Newton equations of motion:

$$\text{(21)} \quad \frac{d}{dt}\left(m\vec{V}\right) = \vec{F}_{FT} + \vec{F}_{Nozzle} + \vec{F}_{Intake} + \vec{F}_G$$

$$\text{(22)} \quad \frac{d}{dt}\left(\overline{\overline{I}}\vec{\omega}\right) = \vec{M}_{FT} + \vec{M}_{Nozzle} + \vec{M}_{Intake} + \vec{M}_G$$

with $\vec{F}_{FT} = \begin{pmatrix} c_{XFT} \cdot q \cdot S \\ c_{YFT} \cdot q \cdot S \\ c_{ZFT} \cdot q \cdot S \end{pmatrix}$ and $\vec{M}_{FT} = \begin{pmatrix} c_{lFT} \cdot q \cdot S \cdot s \\ c_{mFT} \cdot q \cdot S \cdot l_\mu \\ c_{nFT} \cdot q \cdot S \cdot s \end{pmatrix}$.

The inertia tensor I and mass m is modelled by a so-called fuel-rundown loadsheet. This is basically a table, which gives the numbers for inertia and c.g. (under static conditions) as a function of on-board fuel. The aircraft motion ω is measured during flight. Force and moment for the intake F_{Intake}, M_{Intake} and for the nozzle force F_{Nozzle}, M_{Nozzle} of the EJ200 engines is modelled by means of a thrust-in-flight synthetic engine model supplied from Eurojet. This thrust-in-flight deck uses measured parameters, e.g. compressor and turbine speed, pressure and temperature, as input.

The results of (21), (22) are the inertial force and moment F_{FT}, M_{FT}, referenced to the c.g. A translation can be performed by utilising the c.g. position and the force moments.

In parallel model-based force and moment coefficients (c_{XADM}, c_{YADM}, c_{ZADM}, c_{lADM}, c_{mADM}, c_{nADM}) are calculated by putting in parameters such as angel-of-attack, flap positions and flight velocity into the aerodynamic model (ADM). These coefficients are derived in a body-fixed reference frame with the origin in the aerodynamic reference point. The aerodynamic model consists of a multitude of single functions, which describe (the) different aerodynamic effects, e.g. flap effectiveness, interferences between these flaps, influence of the wing-body, influence of the jet efflux, etc. The following functional summarises this as:

$$\text{(23)} \quad \begin{pmatrix} c_{XADM} \\ c_{YADM} \\ c_{ZADM} \end{pmatrix} = \begin{pmatrix} \Im_X(\alpha,\beta,Ma,\delta,...) \\ \Im_Y(\alpha,\beta,Ma,\delta,...) \\ \Im_Z(\alpha,\beta,Ma,\delta,...) \end{pmatrix} = \vec{\Im}$$

$$\text{(24)} \quad \begin{pmatrix} c_{lADM} \\ c_{mADM} \\ c_{nADM} \end{pmatrix} = \begin{pmatrix} \Im_l(\alpha,\beta,Ma,\delta,...) \\ \Im_m(\alpha,\beta,Ma,\delta,...) \\ \Im_n(\alpha,\beta,Ma,\delta,...) \end{pmatrix} = \vec{\Im}$$

4.2. Comparison of the Models with Available Flight Test Data

The quality of the different vortex models can be assessed by comparing the moment coefficients based on the flight test data with results from the vortex model.

$$\delta C_L = \frac{C_{L,model} - C_L}{C_L}$$

$$\text{(25)} \quad \delta C_M = \frac{C_{M,model} - C_M}{C_M}$$

$$\delta C_N = \frac{C_{N,model} - C_N}{C_N}$$

The moment coefficients based on the vortex models can be calculated with the angular rates as follows:

$$C_{L,model} = C_{L0} + C_{L\beta}\beta + C_{Lp}\frac{b}{2V}p_{ind} + C_{Lr}\frac{b}{2V}r_{ind}$$

$$\text{(26)} \quad C_{M,model} = C_{M0} + C_{M\alpha}\alpha + C_{Mq}\frac{c}{2V}q_{ind}$$

$$C_{N,model} = C_{N0} + C_{N\beta}\beta + C_{Np}\frac{b}{2V}p_{ind} + C_{Nr}\frac{b}{2V}r_{ind}$$

The aircraft derivatives were obtained from the aerodynamic model of the *Eurofighter Typhoon*, based on the flight condition measured during the refuelling manoeuvre

The moment coefficients C_{L0}, C_{M0} and C_{N0} are determined by comparing the theoretical moment coefficients to the ones computed with the aerodynamic model based on the flight test data.

$$
\begin{aligned}
& c_{lADM} = C_{L0} + C_L \\
(27)\quad & c_{mADM} = C_{M0} + C_M \\
& c_{nADM} = C_{N0} + C_N
\end{aligned}
$$

The theoretical values for the moment coefficients C_L, C_M and C_N are also computed with the airplane derivatives and the corresponding flight test data.

$$
\begin{aligned}
& C_L = C_{L\xi}\xi + C_{L\zeta}\zeta + C_{L\beta}\beta + C_{Lp}\frac{b}{2V}p_{rel} + C_{Lr}\frac{b}{2V}r_{rel} \\
(28)\quad & C_M = C_{M\alpha}\alpha + C_{M\delta}\delta + C_{M\varepsilon}\varepsilon + C_{M\eta}\eta + C_{Mq}\frac{c}{2V}q_{rel} \\
& C_N = C_{N\xi}\xi + C_{N\zeta}\zeta + C_{N\beta}\beta + C_{Np}\frac{b}{2V}p_{rel} + C_{Nr}\frac{b}{2V}r_{rel}
\end{aligned}
$$

Thus, the moment coefficients can now be directly compared with the moment coefficients computed with the aerodynamic model from the flight test data. The results of this comparison are presented in the following section.

Certain information, which was required for the comparison of the flight test data and the vortex models, was not available in the dataset, especially the position of the receiver aircraft relative to the tanker aircraft. In addition the mass and the angle of attack of the tanker during refuelling was unavailable. For these data assumptions were made based on experience.

5. ASSESSMENT OF THE AERODYNAMIC MODELS

The flight test data are compared to the results of the calculations of the seven different vortex models, each with the five different weighting methods. both with and without the simplification (20). The comparison takes place at three different times of the refuelling process: at the beginning (T_1), in the middle (based on the received fuel; T_2) and at the end of the refuelling (T_3).

The vortex method shall later be used for an automatic refuelling control system. Therefore the requirements for the vortex model to be chosen were twofold. Firstly, both the flight test data and calculations based on the previous models showed, that the tanker's trailing vortex has a negligible influence onto pitching and yawing moments in comparison to the rolling moment. Therefore the vortex model can be chosen by evaluating the rolling moment only. Secondly, the vortex model will be later used to design a control system with a feed-forward control scheme and thereby enable a smoother control. For this application the estimated shall be over- rather than under-estimated. Therefore the two selection criteria for the vortex models were:

- Relative error in pitching and yawing moment coefficients are of second order; quality of the relative error in rolling moment coefficient determines the quality of a model
- The relative error in the rolling moment coefficient must not be negative

Some of the vortex models presented above use parameters like the core radius of the trailing vortex r_c or the vortex parameter ε. As these parameters are only estimated values, the error in the rolling moment coefficient of the selected model shall vary as little as possible around the estimated parameter value.

Presented and discussed here are the relative errors in the rolling moment coefficient at the end of the refuelling process (T_3), for each vortex model with the different weighting methods. In the legend of the presented plots, *iweight=1* to *iweight=5* refers to the five weighing methods 3.2.2.1 to3.2.2.5.

5.1. Results

5.1.1. Horseshoe Vortex Model

The simplest model shows very good results for weighting methods 3.2.2.4 and 3.2.2.5 (c.f. FIG 6). This is remarkable as in an internal study the above mentioned vortex models were used to calculate the down- and sidewash produced by an *Airbus A340-300*. The results were compared to CFD computations where the Horseshoe Vortex Model showed the highest discrepancy.

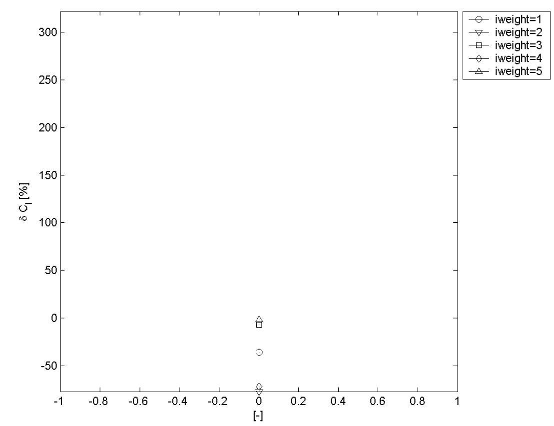

FIG 6. Horseshoe Vortex Model

5.1.2. Hallock-Burnham Vortex Model

The Hallock-Burnham Vortex Model, shown in FIG 7, showed good results for very small values for the core radius r_c for the weighting methods 3.2.2.4 and 3.2.2.5. For increasing values of r_c the relative error in the rolling moment coefficient increases rapidly for all five different weighting schemes.

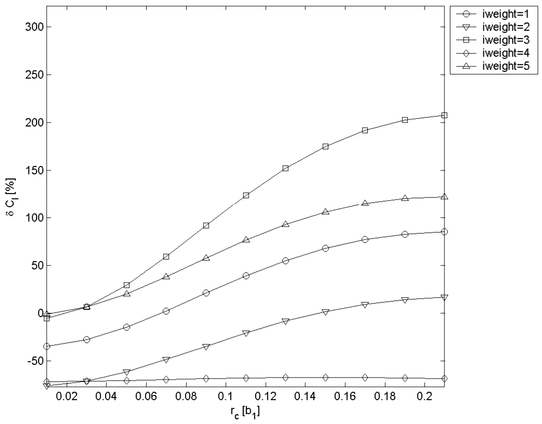

FIG 7. Hallock-Burnham Vortex Model

5.1.3. Lamb-Oseen Vortex Model

The results of the Lamb-Oseen Vortex Model are presented in FIG 8. For the two weighting methods 3.2.2.4 and 3.2.2.5 this model shows very good results for core radii r_c smaller than 0.1 times the wing span of the tanker airplane. For these values, the relative error in the rolling moment coefficient δC_l is independent from r_c. For values higher than r_c*=0.1b* the relative error increases rapidly. The above mentioned comparison of down- and sidewash predicted by the vortex models compared to CFD data showed the best results for r_c *=0.1b*.

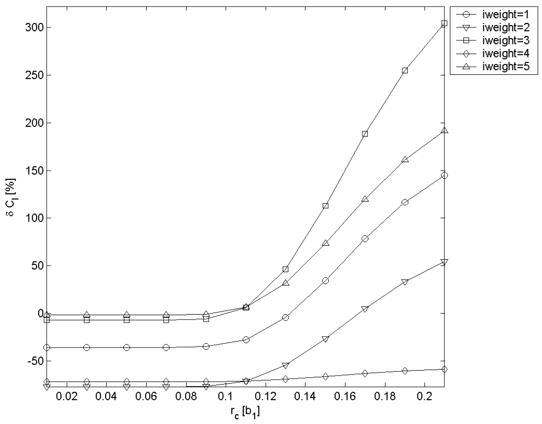

FIG 8. Lamb-Oseen Vortex Model

5.1.4. Modified Horseshoe Vortex Model

The Modified Horseshoe Vortex Model (FIG 9) shows good results for small values of the vortex decay parameter ε by using the either weighting method 3.2.2.4 or 3.2.2.5. The relative error increases for ε>0.04 Venkataramanan and Dogan [7] suggested ε=0.06Γ. For our configuration the down- and sidewash comparison with CFD-data showed the best results for ε=0.15Γ .. 0.20Γ.

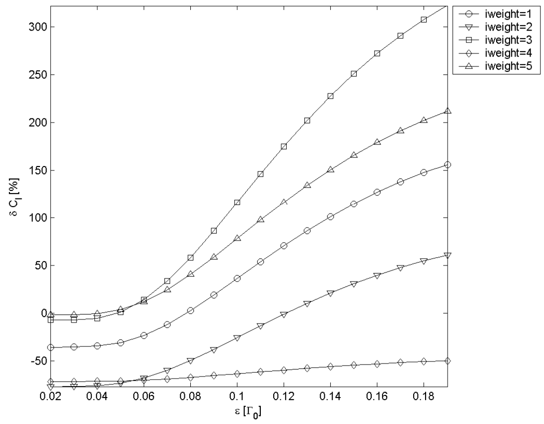

FIG 9. Modified Horseshoe Vortex Model

5.1.5. Rankine Vortex Model

The results of the Rankine Vortex Model compared to the flight test data are presented in FIG 10. For the weighting methods 3.2.2.4 and 3.2.2.5 this vortex model shows very good results, independently of the chosen value for the core radius r_c.

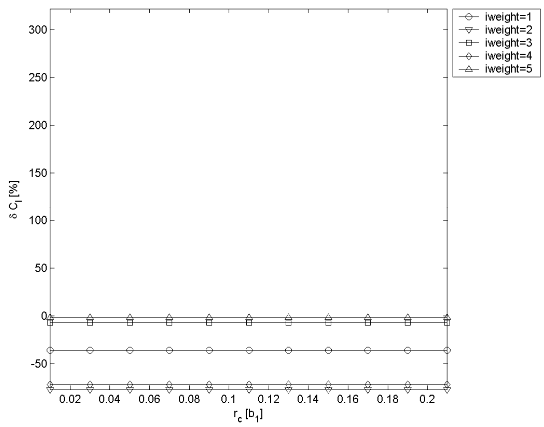

FIG 10. Rankine Vortex Model

5.1.6. Adapted Vortex Model

The Adapted Vortex Model (c.f. FIG 11) also showed good results independently of the chosen value for the core radius r_c for both weighting methods 3.2.2.4 and 3.2.2.5.

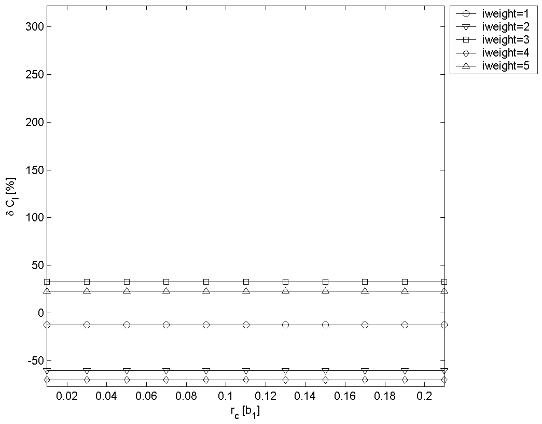

FIG 11. Adapted Vortex Model

5.1.7. Smooth Blending Vortex Model

The results for the Smooth Blending Vortex Model are shown in FIG 12 and FIG 13 for *p=2* and *p=4* respectively. Depending on the parameter p this vortex model shows good results for small values of the core radius r_c. The higher the value of p, the longer the relative error in the rolling moment coefficient δC_l remains independent from the core radius r_c.

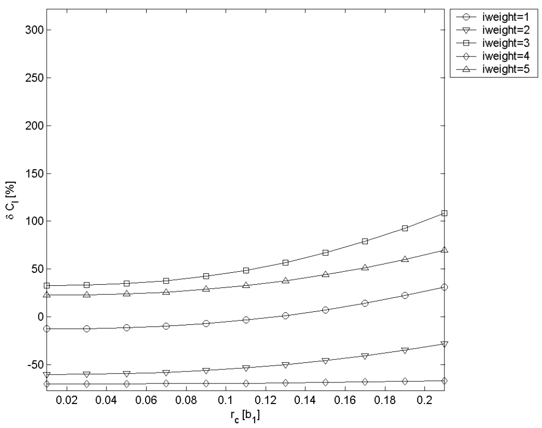

FIG 12. Smooth Blending Vortex Model, p=2

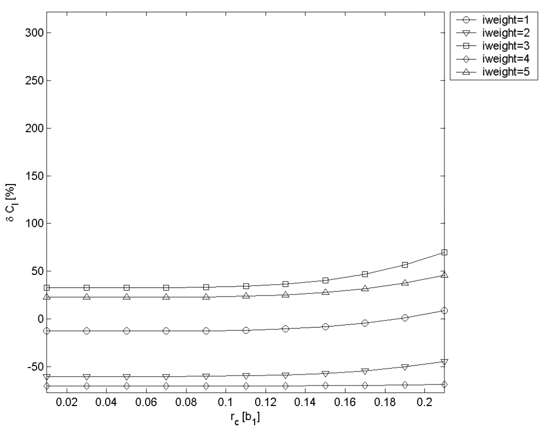

FIG 13. Smooth Blending Vortex Model, p=4

5.2. Assessment of weighting methods

Weighting models 3.2.2.4 and 3.2.2.5 showed the best results throughout all vortex models where the weighting method 3.2.2.5 showed less dependency on the relative error in the rolling moment coefficient δC_l from both vortex parameters, core radius r_c and vortex decay parameter ε.

5.3. Model selection for automatic refuelling control system

The results showed that the quality of the Hallock-Burnham, Lamb-Oseen, Modified Horseshoe and Smooth Blending Vortex Models depend on the selected value of either the core radius r_c or the vortex decay parameter ε. From the results presented above, the appropriate parameter for this specific configuration can be determined. But the comparison, also mentioned above, of the down- and sidewash with another tanker aircraft showed different optimum values. Therefore the suitable value for as well the core radius r_c as for the vortex decay parameter ε apparently depends on the tanker aircraft under consideration

As the potential control system shall, if possible, be independent from the tanker aircraft, these models were not suitable for our purposes.

The remaining models, the Horseshoe, the Rankine and the Adapted Vortex Model did not show this dependency.

In spite of its good results, we did not select the Horseshoe Vortex Model. This is because the other two models both describe the vortex in more detail, and at the same time, require no more computational power. The Rankine Vortex Model showed for the three different points of the refuelling process T_1, T_2 and T_3 a relative error in the rolling moment coefficient between -5 and +100 %, the Adapted Vortex Model between +20 and +125%. As the rolling moment must not be underestimated for control system design, we have chosen the Adapted Vortex Model with Linear Weighting starting from 1 as the most suitable vortex model.

6. CONCLUSION

The flight-mechanic modelling of the interactions between an aerial tanker and a considerably smaller receiving aircraft has been described. Several models for the description of the tanker's trailing vortices are presented. By means of an averaging scheme, these models are then used for determining the additional velocities and angular rates, which are induced at the receiving aircraft's centre of gravity.

Both the flight test data for the aerial refuelling of a modern high-performance aircraft and calculations based on the vortex models showed, that the tanker's trailing vortex has a negligible influence onto pitch and yawing moments in comparison to the rolling moment.
For the rolling moment calculation the Adapted Vortex Models and the Rankine Vortex Model showed sufficiently good results. However, robustness considerations for control law design suggest, that any model should rather over-estimate an effect than under-estimate. Therefore the

Adapted Vortex Models with Linear Weighting starting from 1 is considered the best choice for flight-mechanic considerations and control law design.

REFERENCES

[1] Blake, W.; Dickes, E.; Gingras, D.: UAV Aerial Refuelling – Wind Tunnel Results and Comparison with Analytical Predictions, AIAA Atmospheric Flight Mechanics Conference and Exhibit, 16 - 19 August 2004, Providence, Rhode Island, AIAA-2004-4820

[2] Hansen, J; Murray, J; Campos, N.: The NASA Dryden AAR Project: A Flight Test Approach to an Aerial Refuelling System, AIAA Atmospheric Flight Mechanics Conference and Exhibit, 16 - 19 August 2004, Providence, Rhode Island, AIAA-2004-4939

[3] S. Petersen et al: Development and Testing of the Autonomous Formation Flight Research System, AIAA's 1st Technical Conference and Workshop on Unmanned Aerospace Vehicles, Systems, Technologies, and Operations, 20 -23 May 2002, Portsmouth, Virginia, AIAA-2002-3509

[4] Fravolini, M. L., Ficola, A., Napolitano, M. R., Campa, G., Perhinschi, M. G., “Development of Modeling and Control Tools for Aerial Refueling of UAVs”, AIAA Guidance Navigation and Control Conference 2003, Aug 11-14, 2003 Austin, TX, USA., AIAA 2003-5798

[5] Burnham, D.C. ; Hallock, J.N.: Wake Vortex Decay. Chicago monostatic acoustic vortex sensor system (1982), July, Nr. DOT-TSC-FAA-79-103.IV

[6] Lamb, H.: Hydrodynamics. 6th ed.. New York: Dover, 1923

[7] Venkataramanan, S.; Dogan, A.: Modeling of Aerodynamic Coupling Between Aircraft in Close Proximities. AIAA Atmospheric Flight Mechanics Conference and Exhibit (August 2004), Nr. AIAA-2004-5172

[8] Proctor, F. H.: The NASA-Langley wake vortex modelling effort in support of an operational aircraft spacing system. 36th AIAA Aerospace Sciences Meeting and Exhibit (January 1998), Nr. AIAA 1998-589

[9] Winckelmans, G.; Thirifay, F.; Ploumhans, P.: Effect of non-uniform wind shear onto vortex wakes: parametric models for operational systems and comparison with CFD studies. 4th WakeNet Workshop on „Wake Vortex Encounter“, NLR, Amsterdam, Netherlands (October 2000)